

Spinning instability of gaseous detonations

By **ASLAN R. KASIMOV** AND **D. SCOTT STEWART**†

Theoretical and Applied Mechanics, University of Illinois, 104 S. Wright St.,
Urbana, IL 61801, USA

(Received 29 October 2001 and in revised form 11 March 2002)

We investigate hydrodynamic instability of a steady planar detonation wave propagating in a circular tube to three-dimensional linear perturbations, using the normal mode approach. Spinning instability is identified and its relevance to the well-known spin detonation is discussed. The neutral stability curves in the plane of heat release and activation energy exhibit bifurcations from low-frequency to high-frequency spinning modes as the heat release is increased at fixed activation energy. With a simple Arrhenius model for the heat release rate, a remarkable qualitative agreement with experiment is obtained with respect to the effects of dilution, initial pressure and tube diameter on the behaviour of spin detonation. The analysis contributes to the explanation of spin detonation which has essentially been absent since the discovery of the phenomenon over seventy years ago.

1. Introduction

Spin detonation in gases is one of the forms of multi-dimensional detonation propagation. Its discovery was made by Campbell & Woodhead (1926, 1927). They observed that detonation in tubes of circular cross-section in a stoichiometric mixture of carbon monoxide and oxygen exhibits a highly luminous region which traces a helical path along the periphery of the tube at a nearly constant angular frequency. During its long history the spin phenomenon has been investigated in much detail experimentally using photographic and smoke-foil techniques (see e.g. Voitsekhovskii, Mitrofanov & Topchian 1963; Schott 1965). The structure of the spinning wave close to the wall has been well established and is shown to represent complex Mach configurations consisting of shock and detonation fronts and tangential discontinuities. Only a few studies have been devoted to the study of the spin internal structure. Rigorous theoretical and numerical studies of the spin are lacking, since the spin detonation is inherently three-dimensional and thus challenging. Spinning waves can be observed in slow combustion and their theoretical analyses can be found in the literature: see, for example, Sivashinsky (1981), Matkowsky & Olagunju (1982). Also, spin detonation is frequently observed in two-phase mixtures: see, for example, Zhang & Gronig (1991). In this paper we focus on spin detonation in gases.

The spin is an important regime of multi-dimensional detonation, both from theoretical and practical points of view. From a theoretical perspective it can be considered as one of the manifestations of a cellular detonation. From practical considerations, the importance of knowing the mechanism of spinning detonation stems from the fact that as a mainly marginal phenomenon it is accompanied by

† Author to whom correspondence should be addressed: email dss@uiuc.edu.

localized regions of extremely high pressure (e.g. about $170 p_0$ behind the spin head is reported in Voitsekhovskii *et al.* 1963, where p_0 is the pressure in the fresh mixture). Obviously, such high pressures are to be avoided in many practical systems. Also, in practice detonation waves often occur in some kind of a confinement and instability predictions obtained for detonation in infinite space may have limited applicability to such conditions. In particular, the spinning instability may have relevance to the problem of the pulse-detonation engine which uses detonations that propagate in cylindrical tubes. Therefore it is important to determine the effect of confinement on the instability boundaries. The strategy developed below is for a cylindrical geometry, but following similar ideas rectangular geometry can be handled without difficulty.

Despite the apparent significance of the problem, current understanding of the spin detonation is at the level of qualitative speculations, so there exists a clear need for a detailed look at fundamental mechanisms such as the instability of perturbations to initially steady, planar detonation. It is now well known that for a wide range of parameters one-dimensional detonations are unstable to both one- and two-dimensional linear perturbations (see e.g. Erpenbeck 1964; Lee & Stewart 1990; Bourlioux & Majda 1992, 1995; Short & Stewart 1998). This kind of instability has an important relationship to the cellular structure of multi-dimensional detonations. Except for Pukhnachev's early work (1963), all the existing literature on detonation stability that we are aware of is concerned with detonations extending to infinity in both the longitudinal and lateral directions. Pukhnachev (1963) sets down the modal problem for a detonation in a tube, but makes no mention of spin detonation.

The main phenomenological characteristics of the spin detonation are found in the experimental literature. The structure of the spin detonation was most carefully studied by Voitsekhovskii *et al.* (1963) and independently by Schott (1965). Using photographic and smoke-foil techniques they investigated the complex details of the structure of the spinning front near the wall. The spin structure as proposed by Voitsekhovskii *et al.* (1963) and by Schott (1965) is schematically shown in figure 1(b). The dark bands in figure 1(a), corresponding to the spin head DE in figure 1(b), show schematically the smoke foil records left by a single-head spin detonation. In the case of multiple-head spin, several transverse waves similar to ABCDE exist, which can rotate in opposite directions and interact with each other creating cellular imprints on the soot-foils.

The experiments by Bone, Fraser & Wheeler (1935), and Gordon, Mooradian & Harper (1959) have shown that spin is a near-limit phenomenon occurring mostly in mixtures near their detonability limits. Since the spinning wave moves along a helical path, one of the easily measured characteristics of the spin is the pitch p of the helix, which is the axial advancement of the detonation shock complex for one rotation of the spin head. It was shown that for a given mixture composition the ratio of the pitch to the tube diameter d , i.e. p/d , is independent of the diameter and is about 3 for most mixtures. When the detonation is initiated by a strong source which leads to initial overdrive, it was observed that the occurrence of a spinning wave coincided with the detonation velocity approaching the Chapman–Jouguet (CJ) value. Thus an overdrive is likely to suppress spinning instabilities, like its well-known effect on longitudinal as well as transverse instabilities. Gordon *et al.* (1959) contains extensive measurements of p/d made in hydrogen–oxygen mixtures, either pure or diluted with argon, nitrogen or helium at various initial pressures. In near-limit mixtures p/d was always about 3, while in other mixtures it could take on different values, all ranging between about 2 and 6. An example of a mixture with a high value of p/d is the hydrogen–oxygen mixture diluted with helium at high initial pressures.

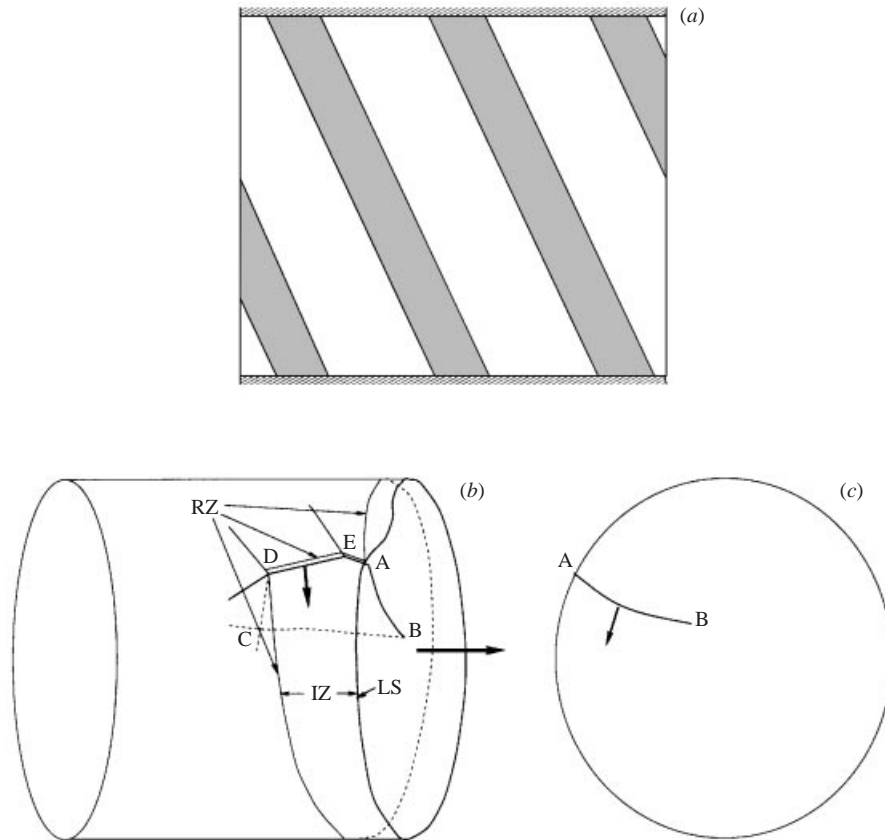


FIGURE 1. (a) Sketch of a soot foil record left by a single-head spin detonation; (b) schematic structure of the spin as proposed in Voitsekhovskii *et al.* (1963) and in Schott (1965): LS – leading shock front, ABCDE – transverse detonation front (spin head), IZ – induction zone, RZ – thin reaction zone behind the lead shock and behind the spin head, AB – the line of triple-shock intersection; (c) the front view of (b). Bold arrows indicate the direction of propagation.

Low initial pressures of a mixture also favour formation of a steady spin. Generally, at low pressures a single spinning front is observed, while an increase in pressure can lead to the formation of several rotating fronts. For example, Duff (1961) observed a single-head spin in a stoichiometric hydrogen–oxygen mixture in a 5/8 in. diameter tube at initial pressure $p_0 = 3.99$ mm Hg, while at $p_0 = 8.49$ mm Hg a diamond-like pattern was observed. As the pressure is increased, the general trend is that the pattern becomes finer and usually very irregular; symmetrical patterns were found to be rather uncommon and unstable. Duff attributes the diamond-shape of the patterns to the interaction of multiple spinning shocks of different helicity, strength and frequency. Duff's investigations also include end-plate soot records which provide certain evidence for the existence of multiple-head spins and their internal structure; the records show that the spin discontinuity extends toward the tube centre and often terminates at roughly half the radius from the wall.

Munday, Ubbelohde & Wood (1968) have investigated the effect of dilution on the spin in hydrogen–oxygen mixtures diluted with argon, $2\text{H}_2 + \text{O}_2 + x\text{Ar}$. In a certain range of argon dilution only a single-head spin was observed, while a decrease

of argon concentration led to the occurrence of a multiple-head spin instead of a single-head spin. Further decreases in the argon content led to a rippled chaotic front.

Manson (1946), Fay (1952), and Chu (1956) independently developed a simple theory which was the best explanation of spin detonation. The basic underlying idea of the theory is the assumption that the spinning detonation front is intimately coupled to the acoustic field in the detonation products. The exact physical mechanism of the coupling is left unexplained, but it is assumed that the frequency of one of the first (typically the first) angular modes of acoustic waves in the tube is equal to the rotation frequency of the spinning front. The CJ detonation model is assumed with uniform profiles of pressure and temperature (except for acoustic perturbations) behind the CJ plane. The solution of the wave equation in a tube involves three eigenvalues which are determined by the boundary conditions at the wall and at the CJ plane. Periodicity is assumed in the azimuthal direction, and the radial velocity vanishes at the wall. An additional boundary condition which is needed to close the problem is the assumption of a planar transverse vibration at the CJ plane. Although no physical justification is given for the latter assumption, they obtain a formula for the pitch-to-diameter ratio that is in rough agreement with experiments:

$$\frac{p}{d} \approx \frac{\gamma_{prod} + 1}{\gamma_{prod}} \frac{\pi}{k_n}. \quad (1)$$

Here k_n is the first root of the derivative of the Bessel function of the first kind. For typical values of the adiabatic exponent γ_{prod} in detonation products, the formula gives a value of about 3 for a single-head spin in close agreement with experimental results. But the theory does not consider the reaction zone which is necessarily involved in the mechanism of spinning instability.

In this work we study instability of the one-dimensional steady detonation in a cylindrical tube subject to three-dimensional linear perturbations by the method of normal modes. The mathematical formulation of the linear instability problem of spin detonation and the solution technique is similar to that by Lee & Stewart (1990) used to describe a one-dimensional instability analysis of gaseous detonations. One of the main differences in the present work from recent past works is the use of cylindrical coordinates. As we will explain, cylindrical coordinates impose a distinct form of the condition at infinity. Also, the analogue to the transverse wavenumber has discrete modes instead of having continuous variation.

In §2 we present the governing equations and the scalings that are used throughout the rest of the paper. Section 3 contains a brief discussion of the steady-state one-dimensional solution. In §4 we present the (linearized) form of the stability equations. In §5 we derive the radiation condition and discuss the variance of the radiation condition with that found for Cartesian coordinates. In §6 we present a very brief discussion of the numerical technique used to find eigenvalues, eigenfunctions and neutral stability curves. In §7 we concentrate on results associated with neutral stability boundaries and how our results are consistent with experimental observations regarding the pitch ratio. Section 8 contains concluding remarks.

2. Governing equations

The governing equations are the Euler equations of gasdynamics for a reactive gas medium, which can be written as

$$\frac{\partial \rho}{\partial t} + \mathbf{u} \cdot \nabla \rho + \rho \nabla \cdot \mathbf{u} = 0, \quad (2)$$

$$\frac{\partial \mathbf{u}}{\partial t} + \mathbf{u} \cdot \nabla \mathbf{u} + \frac{1}{\rho} \nabla p = 0, \quad (3)$$

$$\frac{\partial h}{\partial t} + \mathbf{u} \cdot \nabla h - \frac{1}{\rho} \frac{\partial p}{\partial t} = 0, \quad (4)$$

$$\frac{\partial \lambda}{\partial t} + \mathbf{u} \cdot \nabla \lambda = \omega. \quad (5)$$

The energy equation (4) is written in terms of the total enthalpy $h = e + p/\rho + \mathbf{u}^2/2$, where e is the specific internal energy, p is the pressure, ρ is the density, \mathbf{u} is the velocity, ω is the reaction rate and λ is the reaction progress variable. An Arrhenius simple-depletion form for the reaction rate law and an ideal thermal equation of state are also assumed,

$$e = \frac{1}{\gamma - 1} \frac{p}{\rho} - Q\lambda, \quad \omega = k(1 - \lambda) \exp(-E/RT), \quad p = \rho RT. \quad (6)$$

The energy equation can be rewritten in terms of pressure as

$$\frac{\partial p}{\partial t} + \mathbf{u} \cdot \nabla p + \gamma p \nabla \cdot \mathbf{u} - (\gamma - 1) Q \rho \omega = 0. \quad (7)$$

The normal shock relations for the lead shock must be added to complete the governing equations. We assume that upstream the fluid is motionless with $\mathbf{u} = 0$, and use a 0 subscript to label the upstream ambient state and an s subscript to label the shocked state. Take $v = 1/\rho$ to be the specific volume. Let $\mathbf{D} = D\mathbf{n}$ be the normal shock velocity, where \mathbf{n} is the outward unit normal to the shock. Let unit vectors $\mathbf{t}_1, \mathbf{t}_2$ lie in the tangent plane of \mathbf{n} . Then for the ideal equation of state, with the previous assumptions the shock relations can be written as

$$\left. \begin{aligned} \rho(\mathbf{u} - \mathbf{D}) \cdot \mathbf{n} |_0 &= \rho(\mathbf{u} - \mathbf{D}) \cdot \mathbf{n} |_s = m, & p - p_0 &= m^2(v_0 - v_s), \\ \mathbf{u} \cdot \mathbf{t}_1 |_s &= 0, & \mathbf{u} \cdot \mathbf{t}_2 |_s &= 0, \\ \frac{\gamma}{\gamma - 1} \frac{p_0}{\rho_0} + \frac{\mathbf{D}^2}{2} &= \frac{\gamma}{\gamma - 1} \frac{p_s}{\rho_s} + \frac{(\mathbf{u} - \mathbf{D})^2}{2}, & \lambda_s &= 0. \end{aligned} \right\} \quad (8)$$

Next we scale the variables and develop the dimensionless form for the governing system. Dimensional scales are based on the one-dimensional steady detonation wave. The density, pressure and velocity scales are steady detonation shock density, pressure and sound speed, ρ_s, p_s and c_s . The length scale is chosen to be the steady half reaction zone length, $\ell_{1/2}$, i.e. for a chosen steady detonation, the length behind the shock for the reaction progress variable to reach one half. The time scale is the length scale divided by the velocity scale, $\ell_{1/2}/c_s$. To simplify our notation we now use a tilde to represent dimensional quantities, a plain variable to represent dimensionless quantities, an asterisk to identify quantities of the one-dimensional steady state and b subscript to refer to the states at the end of the reaction zone.

3. The one-dimensional steady state

The one-dimensional steady state is found simply from integrating the conservative form of the governing equations in a frame moving with the detonation, which gives the ZND detonation structure. We follow the presentation found in Lee & Stewart (1990) and the results are given again for convenience. If u^* is the particle velocity in the steady frame, and p^* and ρ^* are the steady pressure and density, these are

expressed in terms of λ^* by

$$p^* = a + (1 - a)\sqrt{1 - b\beta\lambda^*}, \quad u^* = \frac{1 - p^*}{\gamma M_s} + M_s, \quad \rho^* = \frac{M_s}{u^*}, \quad (9)$$

where $M_s = \tilde{u}_s^*/\tilde{c}_s^*$ is the Mach number behind the shock as seen from an observer riding the shock. It is useful to introduce $D = \tilde{D}^*/\tilde{c}_0$ to represent the steady Mach number of the detonation relative to an observer in the ambient material or lab-frame. The constants a and b , and the relationship between M_s and D are given by

$$a = \frac{1 + \gamma M_s^2}{\gamma + 1}, \quad b = \frac{2\gamma(\gamma - 1)M_s^2}{(\gamma + 1)(1 - a)^2}, \quad M_s^2 = \frac{2 + (\gamma - 1)D^2}{2\gamma D^2 - (\gamma - 1)}. \quad (10)$$

At the shock front the steady-state variables satisfy

$$\rho^* = 1, \quad p^* = 1, \quad u^* = M_s, \quad \lambda^* = 0. \quad (11)$$

The dimensionless heat release and the activation energy are defined as $\beta = \gamma\tilde{Q}/(\tilde{c}_s^*)^2$ and $\Theta = \gamma\tilde{E}/(\tilde{c}_s^*)^2$ respectively. While it is convenient to carry out the analysis in post-shock scales, the effect of the scaling is to make the scales dependent on the reaction zone length and in particular the activation energy. Many results of simulations are reported for activation energy and heat release scaled with respect to the upstream condition (Erpenbeck's scales). Plain E is used to represent the scaled activation energy $E = \gamma\tilde{E}/\tilde{c}_0^2$ and plain Q is used to represent the scaled heat release $Q = \gamma\tilde{Q}/\tilde{c}_0^2$.

The overdrive factor is defined as $f = (D/D_{CJ})^2$ where $D_{CJ} = \tilde{D}^*/\tilde{c}_0$ is the scaled Chapman–Jouguet detonation velocity given by the formula

$$D_{CJ} = \sqrt{1 + \frac{(\gamma^2 - 1)Q}{2\gamma}} + \sqrt{\frac{(\gamma^2 - 1)Q}{2\gamma}}. \quad (12)$$

The spatial structure of λ^* is obtained by integration of the rate equation as

$$z = \int_0^{\lambda^*} \frac{u^*(\lambda)}{\omega^*(\lambda)} d\lambda = \frac{1}{k} \int_0^{\lambda^*} \frac{u^*(\lambda)}{1 - \lambda} e^{\Theta/(p^*/\rho^*)} d\lambda. \quad (13)$$

The value of $k = \tilde{k}\tilde{\lambda}_{1/2}^*/\tilde{c}_s^*$ is fixed by setting $z = 1$ when $\lambda^* = 1/2$ in the above integral.

4. The linear stability problem

Here we present the formulation of the linear stability problem that determines the normal modes. We use cylindrical coordinates attached to the perturbed shock front. The superscript l is used to indicate variables $(r^l, \theta^l, z^l, t^l)$ represented in the laboratory frame. Let $D_s = \tilde{D}^*/\tilde{c}_s^*$ be the steady detonation shock velocity scaled by the steady post-shock sound speed. Next we introduce the shock-attached coordinates (r, θ, z, t) through the coordinate transformation

$$z = z^l - D_s t^l - \psi(r^l, \theta^l, t^l), \quad r = r^l, \quad \theta = \theta^l, \quad t = t^l. \quad (14)$$

The function ψ represents the shock front displacement from the unperturbed position. The instantaneous location of the shock front is at $z = 0$ in the shock-attached coordinates. Note that the velocity of the shock-attached frame is $D_s + \partial\psi/\partial t$, hence the particle velocity in the frame is $u_z = u_z^l - D_s - \partial\psi/\partial t$. This choice is consistent with the definition of u_z found in the detonation shock dynamics studies that use intrinsic

shock-attached coordinates, where the shock acceleration of the frame explicitly appears in the governing equations, see for example, Yao & Stewart (1996). In previous linear stability works such as Lee & Stewart (1990) and Short & Stewart (1998), the particle velocity in the steady frame, $u'_z - D_s$ (not the z velocity component in the shock-attached frame) is used instead as the dependent z velocity component, which follows Erpenbeck's earlier precedent. The formulation here differs slightly, and the shock relations, in particular are affected. However either choice could have been made without any effect on the conclusions.

If we introduce the operators Φ and L defined by

$$\Phi \equiv u_r \frac{\partial \psi}{\partial r} + \frac{u_\theta}{r} \frac{\partial \psi}{\partial \theta}, \quad L \equiv u_r \frac{\partial}{\partial r} + \frac{\partial u_\theta}{\partial r} \frac{\partial}{\partial \theta} + (u_z - \Phi) \frac{\partial}{\partial z}, \quad (15)$$

then the transformed set of the governing equations becomes

$$\frac{\partial \rho}{\partial t} + \mathbf{u} \cdot \nabla \rho + \rho \nabla \cdot \mathbf{u} - \frac{\partial \rho \Phi}{\partial z} = 0, \quad (16)$$

$$\frac{\partial u_r}{\partial t} + L(u_r) - \frac{u_\theta^2}{r} + \frac{1}{\gamma \rho} \frac{\partial p}{\partial r} - \frac{1}{\gamma \rho} \frac{\partial \psi}{\partial r} \frac{\partial p}{\partial z} = 0, \quad (17)$$

$$\frac{\partial u_\theta}{\partial t} + L(u_\theta) + \frac{u_r u_\theta}{r} + \frac{1}{\gamma \rho r} \frac{\partial p}{\partial \theta} - \frac{1}{\gamma \rho r} \frac{\partial \psi}{\partial \theta} \frac{\partial p}{\partial z} = 0, \quad (18)$$

$$\frac{\partial u_z}{\partial t} + L(u_z) + \frac{1}{\gamma \rho} \frac{\partial p}{\partial z} + \frac{\partial^2 \psi}{\partial t^2} = 0, \quad (19)$$

$$\frac{\partial p}{\partial t} + L(p) + \gamma p \nabla \cdot \mathbf{u} - (\gamma - 1) \beta \rho r - \gamma p \frac{\partial \Phi}{\partial z} = 0, \quad (20)$$

$$\frac{\partial \lambda}{\partial t} + L(\lambda) = \omega. \quad (21)$$

Here $\mathbf{u} = (u_r, u_\theta, u_z)$, and in cylindrical polar coordinates, $\mathbf{u} \cdot \nabla = u_r \partial / \partial r + (u_\theta / r) \partial / \partial \theta + u_z \partial / \partial z$ and $\nabla \cdot \mathbf{u} = \partial u_r / \partial r + u_r / r + (1/r) \partial u_\theta / \partial \theta + \partial u_z / \partial z$.

The governing equations can also be written in a matrix form. Let the column vector $\mathbf{q} = [\rho, u_r, u_\theta, u_z, p, \lambda]^T$. Then the equations in the shock-attached frame can be recast as

$$\frac{\partial \mathbf{q}}{\partial t} + \mathbf{A}_z \cdot \frac{\partial \mathbf{q}}{\partial z} + \mathbf{A}_r \cdot \frac{\partial \mathbf{q}}{\partial r} + \mathbf{A}_\theta \cdot \frac{1}{r} \frac{\partial \mathbf{q}}{\partial \theta} + \frac{\mathbf{a}}{r} - \mathbf{B}_r \cdot \frac{\partial \mathbf{q}}{\partial z} \frac{\partial \psi}{\partial r} - \mathbf{B}_\theta \cdot \frac{\partial \mathbf{q}}{\partial z} \frac{1}{r} \frac{\partial \psi}{\partial \theta} + \mathbf{b} \frac{\partial^2 \psi}{\partial t^2} = \mathbf{c}, \quad (22)$$

where the matrices and column vectors are written out in Appendix A. If the equations were steady and plane, then the governing equations would simply be $\mathbf{A}_z \cdot \partial \mathbf{q} / \partial z = \mathbf{c}$.

The equations are expanded about the steady-state solution and we seek solutions to the normal mode of the form

$$\mathbf{q} = \mathbf{q}^*(z) + \mathbf{q}' \exp(\alpha t + in\theta), \quad \psi = \psi' \exp(\alpha t + in\theta), \quad (23)$$

where the prime superscript implies a small amplitude in a norm associated with the deviation of the initial conditions from those of plane steady detonation. A straightforward expansion of the various terms found in (22) combined with the fact that the steady state only depends on z leads to

$$\begin{aligned} \alpha \mathbf{q}' + \mathbf{A}_z^* \cdot \frac{\partial \mathbf{q}'}{\partial z} + \mathbf{A}_r^* \cdot \frac{\partial \mathbf{q}'}{\partial r} + in \mathbf{A}_\theta^* \cdot \frac{1}{r} \mathbf{q}' + \mathbf{A}_z^* \cdot \frac{\partial \mathbf{q}^*}{\partial z} \\ + \frac{\mathbf{a}'}{r} - \mathbf{B}_r^* \cdot \frac{\partial \mathbf{q}^*}{\partial z} \frac{\partial \psi'}{\partial r} - in \mathbf{B}_\theta^* \cdot \frac{\partial \mathbf{q}^*}{\partial z} \frac{1}{r} \psi' + \alpha^2 \mathbf{b}^* \psi' = \mathbf{c}'. \end{aligned} \quad (24)$$

Since all the perturbations are uniformly the same order ($O(\epsilon)$ say) we can now consider the primed variables to be the $O(1)$ coefficient functions.

Then the normal modes are separable in r, θ, z by writing

$$\mathbf{q}' = \begin{bmatrix} \rho'(z)J_n \\ u_r'(z)dJ_n/dr \\ u_\theta'(z)J_n/r \\ u_z'(z)J_n \\ p'(z)J_n \\ \lambda'(z)J_n \end{bmatrix} \quad \text{and} \quad \psi' = J_n. \quad (25)$$

Here $J_n = J_n(kr)$ is the Bessel function of the first kind of integer index n , k is the radial wavenumber to be determined from the boundary condition at the wall and α is a complex growth rate of perturbations.

It follows from the above form of the normal modes that the u_r and u_θ equations yield the relationship

$$u_\theta' - inu_r' = C \exp\left(-\alpha \int_0^z \frac{dz}{u_z^*}\right),$$

where the constant C when found from Rankine–Hugoniot conditions (which imply $u_\theta'(0) = inu_r'(0)$) turns out to be zero. Thus

$$u_\theta'(z) = inu_r'(z) \quad (26)$$

and once the u_r' perturbation is found u_θ' follows directly. Thus the system of complex ODEs is reduced from six to five. Without loss of generality we can take the shock displacement perturbation amplitude normalized to 1, once we obtain the linearized equations, since the eigenfunctions are determined up to a multiplicative constant.

The stability equations can be re-written in terms of a new column vector, $\mathbf{f}' = [\rho', u_r', u_z', p', \lambda']^T$, representing the complex perturbations, as follows:

$$\alpha \mathbf{f}' + \mathbf{A}^* \cdot \frac{d\mathbf{f}'}{dz} + \mathbf{C}^* \cdot \mathbf{f}' + \mathbf{b}^* = 0, \quad (27)$$

where \mathbf{A}^* , \mathbf{C}^* and \mathbf{b}^* are given by

$$\mathbf{A}^* = \begin{bmatrix} u_z & 0 & \rho & 0 & 0 \\ 0 & u_z & 0 & 0 & 0 \\ 0 & 0 & u_z & 1/(\gamma\rho) & 0 \\ 0 & 0 & \gamma p & u_z & 0 \\ 0 & 0 & 0 & 0 & u_z \end{bmatrix}^*, \quad \mathbf{b}^* = \begin{bmatrix} 0 \\ -p_{,z}/(\gamma\rho) \\ \alpha^2 \\ 0 \\ 0 \end{bmatrix}^*, \quad (28)$$

$$\mathbf{C}^* = \begin{bmatrix} u_{z,z} & -k^2\rho & \rho_{,z} & 0 & 0 \\ 0 & 0 & 0 & 1/(\gamma\rho) & 0 \\ -1/(\gamma\rho^2)p_{,z} & 0 & u_{z,z} & 0 & 0 \\ -(\gamma-1)\beta(\omega + \rho\omega_{,\rho}) & -\gamma k^2 p & p_{,z} & \gamma u_{z,z} - (\gamma-1)\beta\rho\omega_{,p} & -(\gamma-1)\beta\rho\omega_{,\lambda} \\ -\omega_{,\rho} & 0 & \lambda_{,z} & -\omega_{,p} & -\omega_{,\lambda} \end{bmatrix}^*. \quad (29)$$

Note that \mathbf{A}^* follows directly from the definition of \mathbf{A}_z^* . The matrix \mathbf{C}^* has contributions from all the other \mathbf{A}^* terms. The term \mathbf{b}^* is determined from the shock

displacement. The reaction rate sensitivities are defined by the expansion of the reaction rate as $\omega' = \omega_{,p}^* p' + \omega_{,\rho}^* \rho' + \omega_{,\lambda}^* \lambda'$, where $\omega_{,p}^* = \Theta \rho^* \omega^* / (p^*)^2$, $\omega_{,\rho}^* = -\Theta \omega^* / p^*$, and $\omega_{,\lambda}^* = -\omega^* / (1 - \lambda^*)$. Notice, that there is no singularity in the system at any point, except for the CJ case, for which one of the eigenvalues of \mathbf{A}^* becomes zero at infinity. The CJ case is treated by a limit as the overdrive factor f approaches 1.

The Rankine–Hugoniot relations (8) are expanded to obtain the conditions at the shock, which is located at $z = 0$. Their linearization (with $\psi' = 1$) leads to

$$\left. \begin{aligned} \rho' &= -\frac{4}{(\gamma + 1)D^2 M_s} \alpha, & u'_z &= \frac{2 - (\gamma - 1)D^2}{(\gamma + 1)D^2} \alpha, & u'_r &= -\frac{1}{M_s} \frac{M_s^2 - D^2}{1 + \gamma D^2}, \\ p' &= -\frac{4\gamma M_s}{\gamma + 1} \alpha, & \lambda' &= 0. \end{aligned} \right\} \quad (30)$$

The boundary condition at the tube wall is that the radial velocity is zero, $u_r(r = a) = 0$, where a is the tube radius. It follows then that

$$\left. \frac{dJ_n(kr)}{dr} \right|_{r=a} = 0. \quad (31)$$

Equation (31) determines all possible wavenumbers $k = 2x_{nm}/d$, where $J'_n(x_{nm}) = 0$, for integer $n = 0, 1, 2, \dots$ and $m = 1, 2, \dots$ (Note that negative n (counter-clockwise spin) are also admitted, but since the eigenvalues α would be the same as for corresponding positive n , all conclusions are valid for both clock- and counter-clockwise spins.) In what follows, n will be identified with the number of spin heads, while m is the radial mode number such that $m - 1$ gives the number of zeros of the Bessel function on $0 < r < a$. Note that the eigenfunctions given by $J_0(kr)$ correspond to axisymmetric disturbances with $u'_\theta = 0$ and $\partial/\partial\theta = 0$. An important special case is that of a one-dimensional disturbance corresponding to $k = 0$. It satisfies the wall boundary condition at all a since $J'_0(0) = 0$. Thus our normal modes include not only spinning modes, but also axisymmetric non-spinning as well as purely longitudinal modes.

5. The radiation condition

One more condition is required to close the above system of ODEs and derive the dispersion relation. It is derived from the condition that the initial perturbations are uniformly bounded in space. Spatial unboundedness of unstable eigenfunctions can result from the behaviour of the solution at $z \rightarrow -\infty$. Hence the necessary condition is identified by considering the linearized system in the rear far field where the steady flow is constant and the reaction is complete. An alternative interpretation of the radiation condition is that the intrinsic instability of the detonation is a result of interaction between the leading shock and the reaction zone only and should not be affected by disturbances that travel toward the shock from an infinite distance behind the reaction zone. Hence it is assumed that the disturbance eigenfunctions are missing the incoming wave family at the end of the reaction zone. In one form or another, such a condition has been used by many researchers investigating stability of detonation waves (e.g. Erpenbeck 1962; Buckmaster & Ludford 1989; Lee & Stewart 1990). The radiation condition has a different form in cylindrical coordinates than in Cartesian coordinates, but it expresses the same physical condition. Note that it is possible to apply different conditions, such as for example the piston condition $u' = 0$ at infinity, but it should be realized that as a result, the instability spectrum would be altered by the extra interactions of the piston and leading shock compared to that of the intrinsic mechanism.

Next, we turn to the derivation of the radiation condition in cylindrical coordinates. At the end of the reaction zone where the steady solution reaches a constant state we can set $\lambda' = 0$ because of the reaction rate being negligible and λ' decaying exponentially with increasing z . This assumption does not change the overall result and in Appendix B, we derive the form of the radiation condition where λ' is retained. The acoustic solution in the far field has the same radial dependences as in the normal mode representation in the main flow. But the dependence on time and the axial coordinate are kept arbitrary.

With these assumptions the acoustic expansion is of the general form $\mathbf{q} = \mathbf{q}_b + \hat{\mathbf{q}}$ where the hat refers to an acoustic perturbation. The u_r, u_z and p equations define the acoustic modes and are given by

$$\mathcal{L}\hat{u}_r + \frac{\hat{p}}{\gamma\rho_b} = 0, \quad (32)$$

$$\mathcal{L}\hat{u}_z + \frac{1}{\gamma\rho_b} \frac{\partial \hat{p}}{\partial z} = 0, \quad (33)$$

$$\mathcal{L}\hat{p} + \gamma p_b \left(\frac{\partial \hat{u}_z}{\partial z} - k^2 \hat{u}_r \right) = 0, \quad (34)$$

where $\mathcal{L} \equiv \partial/\partial t + u_b \partial/\partial z$ and the subscript b denotes the burnt state at $z \rightarrow -\infty$. (Equation (33) should have the term $\partial^2 \psi/\partial t^2$ on the left-hand side, but since $\partial^2 \psi/\partial t^2 = \mathcal{L}(\partial \psi/\partial t)$, that term is temporarily absorbed into \hat{u}_z). If we apply the operator \mathcal{L} on equation (34) and make use of equations (32) and (33), then we obtain a single equation in \hat{p} :

$$\frac{\partial^2 \hat{p}}{\partial t^2} + 2u_b \frac{\partial^2 \hat{p}}{\partial t \partial z} - (c_b^2 - u_b^2) \frac{\partial^2 \hat{p}}{\partial z^2} + (c_b k)^2 \hat{p} = 0. \quad (35)$$

This is a Klein–Gordon equation, solutions of which represent dispersive travelling waves. In terms of the characteristic variables $\xi = z - (u_b + c_b)t$ and $\eta = z - (u_b - c_b)t$ it can also be written as $\partial^2 \hat{p}/\partial \xi \partial \eta - (k^2/4)\hat{p} = 0$.

We look for a solution of equation (35) which is of the travelling wave form $\exp(\alpha t + s z)$. Substituting $\hat{p} = \exp(\alpha t + s z)$ into equation (35) we obtain a dispersion relation for the complex axial wavenumber $s(\alpha)$,

$$\alpha^2 + 2u_b \alpha s - (c_b^2 - u_b^2) s^2 + c_b^2 k^2 = 0, \quad (36)$$

which has roots given by

$$s = \frac{1}{c_b^2 - u_b^2} (\alpha u_b + c_b [\alpha^2 + k^2 (c_b^2 - u_b^2)]^{1/2}). \quad (37)$$

Note that in the Chapman–Jouguet limit, $f = 1$ and $D = D_{CJ}$ and it follows that the flow state at the end of the reaction zone is sonic with $c_b = -u_b$, and (37) reduces to

$$s = -\frac{1}{2u_b} \left(\alpha + \frac{c_b^2 k^2}{\alpha} \right). \quad (38)$$

The far-field dispersion relation has two branches of the square root in (37) so that the unstable disturbances with $\text{Re}(\alpha)$ are spatially bounded only if the branch with positive real part is kept. From the travelling-wave character of solutions to the Klein–Gordon equation it is clear that the boundedness requirement is equivalent to elimination of acoustic waves propagating from $z \rightarrow -\infty$ toward the shock.

It is worth pointing out that the situation is not different in principle if we consider the case with a finite reaction zone. Even though the reaction zone does not extend to infinity, and the spatial unboundedness is of no concern anymore, the radiation condition is imposed based on the physics of the problem: the development of unstable perturbations has to occur only due to the interaction between the lead shock front and the reaction zone. The boundary value problem should now be set up for a finite domain and the radiation condition be applied at the end of the reaction zone.

Equation (34) can be rearranged as

$$k^2 \hat{u}_r = \frac{\alpha + u_b s}{\gamma p_b} \hat{p} + \frac{\partial \hat{u}_z}{\partial z}. \quad (39)$$

The time dependence of all the variables has to be the same as in (23), i.e. exponential. The axial dependence is known only upon the solution of the exact normal mode system, but it has to satisfy the above equation (39). Now, writing s in terms of α from (37) and inserting $\hat{p} = p'(z) \exp(\alpha t)$, $\hat{u}_z = u'_z(z) \exp(\alpha t)$, $\hat{u}_r = u'_r(z) \exp(\alpha t)$ into (39) we obtain the *radiation condition*

$$\frac{du'_z}{dz} - k^2 u'_r + \frac{\alpha c_b + u_b [\alpha^2 + k^2 (c_b^2 - u_b^2)]^{1/2}}{\gamma \rho_b c_b (c_b^2 - u_b^2)} p' = 0. \quad (40)$$

By choosing the positive branch of the square root in this equation we explicitly eliminate incoming waves at infinity. Note that for CJ detonation the radiation condition becomes

$$\frac{du'_z}{dz} - k^2 u'_r + \frac{\alpha - k^2 c_b^2 / \alpha}{2\gamma \rho_b c_b^2} p' = 0. \quad (41)$$

Also, for the one-dimensional case, letting $k \rightarrow 0$ we integrate (40) and noting that $\int p' dz = \text{const} \int \exp(sz) dz = p'/s$, we obtain the one-dimensional radiation condition given, for example, in Lee & Stewart (1990) with λ' set to 0,

$$u'_z + \alpha + \frac{1}{\gamma \rho_b c_b} p' = 0. \quad (42)$$

The extra term α in this equation is due to the definition of the axial velocity which is different from that in Lee & Stewart (1990). If u_z^{LS} denotes the axial velocity in Lee & Stewart (1990), then $u_z^{LS} = u_z + \partial \psi / \partial t$ and α in (42) comes from $\partial \psi / \partial t$, i.e. $\int (du'_z / dz) dz = u'_z + \alpha$.

6. The numerical solution and techniques for finding roots

The unstable eigenvalues are found by solving the radiation condition (40) numerically by means of the DNSQE subroutine from NIST mathematical software repository (2001). The subroutine solves a system of nonlinear equations by the Powell hybrid method, a version of the Newton method. To provide the subroutine with an initial guess we first determine the approximate location of the roots of (40) by plotting the magnitude of the left-hand side of (40) (let us denote it H) in some bounded domain of the complex plane α . This is the 'carpet search' method, first introduced by Lee & Stewart (1990) to find the eigenvalues for the one-dimensional detonation. The surface of $|H|$ has clear domains of attraction at the locations of the roots, thus allowing one to obtain the guess from the contour plot of $|H|$. Once the guess is supplied to DNSQE, the subroutine then finds the exact value within a given tolerance (typically $10^{-6} - 10^{-8}$) iteratively. At each iteration the entire solution of the

ODEs (27) is required. The latter is obtained by means of the DDASSL subroutine developed by L. Petzold, which can be found at NIST (2001). This subroutine is based on Gear's method for stiff differential-algebraic systems. The solution for the ODEs is again obtained within a given tolerance, which is typically $10^{-8} - 10^{-10}$. Such accuracy is necessary in order to achieve proper convergence for the root solver. This is because of the property of the radiation condition that the domains of attraction of the roots are extremely small, especially at high frequencies; thus large steps during iterations can keep the solver wandering around the root or make it leave the domain entirely. The efficiency of DNSQE and DDASSL for a similar class of problems was demonstrated by Short & Stewart (1998).

The neutral stability curves are constructed using the arclength continuation method. In this method each subsequent point on the curve is found over a fixed length along the curve. This method avoids numerical difficulties associated with turning points.

7. Discussion of results for spinning instability

Low-frequency spin (i.e. spin detonation with small number of rotating fronts) is typically observed in experiments with explosive mixtures close to their detonability limits (usually lean limits) so that the heat effect Q is small compared to that of a stoichiometric composition. This is the main reason for our focus on the range of Q between 0 and 20 in the following calculations. Small Q implies that the detonation speed and therefore post-shock temperature is small. Strong dependence of the reaction rate on the post-shock temperature leads to a significant increase in the induction-zone length. As the degree of dilution decreases, the number of spin heads is observed to grow. For example, in hydrogen–oxygen–argon mixtures, Munday *et al.* (1968) found that a single-head spin exists within the range of dilution between 88.8 and 91.9 volume percent of argon, while in the range between 87.0 and 88.8 percent a four-head spin was observed, bifurcating from the single-head mode at 88.8 percent argon. Two- and three-head spins were not observed.

We next discuss some of the results of the stability analysis and try to relate them to the above-mentioned experimental findings. Note that the set of bifurcation parameters is composed of the heat release Q , activation energy E , overdrive factor f , adiabatic exponent γ , and the radial wavenumber k (recall that $k \equiv 2x_{nm}/d$, where x_{nm} is the m th root of the Bessel function's derivative, $J'_n(x_{nm}) = 0$, d is the tube diameter, n is the number of maxima in the angular direction (number of spinning heads), $m - 1$ gives the number of nodes of $J_n(kr)$ along the radius; thus $2\pi/k$ is the characteristic wavelength in the radial direction). In this paper we do not attempt to cover the entire space of bifurcation parameters, but rather focus on the detailed analysis of some of them, choosing others on the basis of experimental knowledge about spin detonation. In particular, we keep f fixed at $f = 1.0$, since the experiment indicates that overdrive tends to suppress spin detonation. Also, we look at only two values of the adiabatic exponent, $\gamma = 1.3$ and $\gamma = 1.6$ and two values of the tube diameter, $d = 2$ and $d = 20$ (recall that the length scale is the half-reaction length $\tilde{l}_{1/2}$, so that these tube diameters are twice and twenty times the length of the reaction zone, respectively). We do vary Q and E since Q is related to the degree of dilution (the higher the degree of dilution the smaller heat effect Q), and different E represent mixtures of different reactivity. We vary n and m since these provide a selection of particular modes of spin and, which is very important for the link between the instability results and experiment, give us the spin pitch to diameter ratio p/d for the most unstable mode. Finally, we

$m \setminus n$	1	2	3	4	5	6	7
1	1.841	3.054	4.201	5.318	6.416	7.501	8.578
2	5.331	6.706	8.015	9.282	10.520	11.735	12.932
3	8.536	9.969	11.346	12.682	13.987		

TABLE 1. First few roots of $J'_n(x_{nm}) = 0$.

calculate the dependence of the neutrally stable roots on the radial wavenumber k . This lets us avoid calculating the huge number of discrete modes, labelled with three indices: n , m , each running from one to infinity, as well as the mode index j in the temporal spectrum, which can be as large as tens or even hundreds (j labels the roots α of the radiation condition according to their frequency; for example, $j = 1$ is the lowest frequency root, $j = 2$ is the second lowest frequency root and so on).

First, let us consider the case with fixed values of $d = 20$, $\gamma = 1.6$ and $f = 1.0$. These choices are motivated by the following facts from experiments as well as our own calculations of one-dimensional detonation instability. Experiments show that typical cell size of cellular detonation is of the order of 10 to 100 reaction-zone lengths (see e.g. Fickett & Davis 1979), so that we expect the radial wavenumber for the most unstable mode to be around 0.06 – 0.6. For $d = 20$, the smallest wavenumber is $k = 2x_{11}/d = 0.184$ (see table 1).

The choice of $\gamma = 1.6$ is motivated, first, by the experimental results from Gordon *et al.* (1959) in which the experiments were carried out mostly in hydrogen–oxygen mixtures diluted with monatomic inert gases, such as helium and argon, which render large γ for the mixture (pure helium or argon have $\gamma = 1.67$); secondly, our calculations of one-dimensional instability for various γ indicate that higher γ tends to strongly stabilize detonations with larger Q while destabilizing, albeit insignificantly, detonations at smaller Q , as shown in figure 2. The remaining choice, for $f = 1.0$, is motivated again by experimental reports such as those in Gordon *et al.* (1959), which show that the emergence of spin detonation is most frequent at CJ velocities. This limit is achieved by computing for values of f close, but not exactly equal, to 1, namely $f = 1.01$. In fact, the limit $f \rightarrow 1$ is well behaved in the sense that the solution for the governing equations converges to a limit, although extremely slowly as f becomes closer to 1. There is no appreciable difference in the results between $f = 1.01$ and say $f = 1.0001$, but the latter is prohibitively time-consuming computationally. Also, we did carry out calculations for $\gamma = 1.3$ and $d = 2$, although in less detail than for the case with $\gamma = 1.6$ and $d = 20$, and they reveal some additional features of detonation instability which we shall discuss below.

Figures 3(a) and 3(b) show the neutral stability curves for several spinning modes, ranging from $n = m = 1$ to $n = 10$, $m = 1$ which corresponds to the range of the radial wavenumber k from $k = 0.184$ to $k = 1.189$. In figure 3(a), the leftmost boundary (the left-hand solid line) is composed of three neutral stability curves, namely $n = 3$, $m = 1$ below $Q = 16.1$ and $n = 4$, $m = 1$ or $n = 1$, $m = 2$ above $Q = 16.1$. Similarly, in figure 3(b) the leftmost boundary consists of $n = 3$, $m = 1$ below $Q = 0.69$ (dashed line), $n = 4$, $m = 1$ or $n = 1$, $m = 2$ from $Q = 0.69$ to $Q = 8.5$ and $n = 5$, $m = 1$ from $Q = 8.5$ to $Q = 20$. The thick solid line on both figures is the one-dimensional neutral stability boundary corresponding to $k = 0$. The horizontal dashes indicate the bifurcation points. The dotted lines in both figures correspond to several neighbouring modes below and above the ones which comprise the leftmost boundary. To avoid

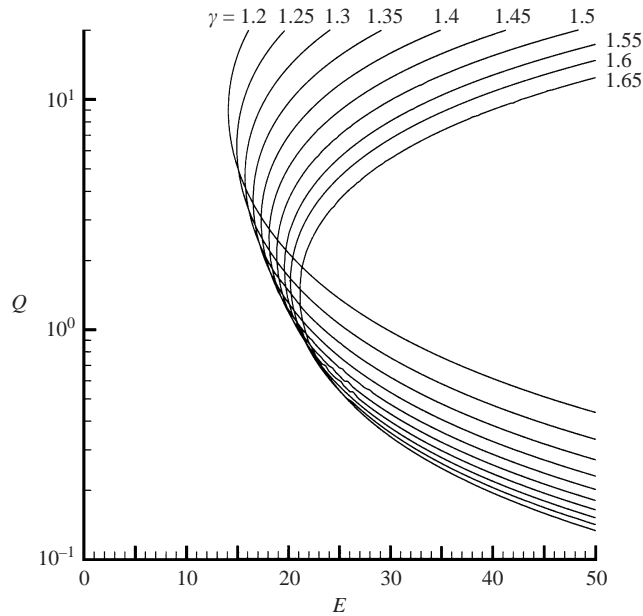


FIGURE 2. The effect of the adiabatic exponent γ on the one-dimensional neutral stability boundary.

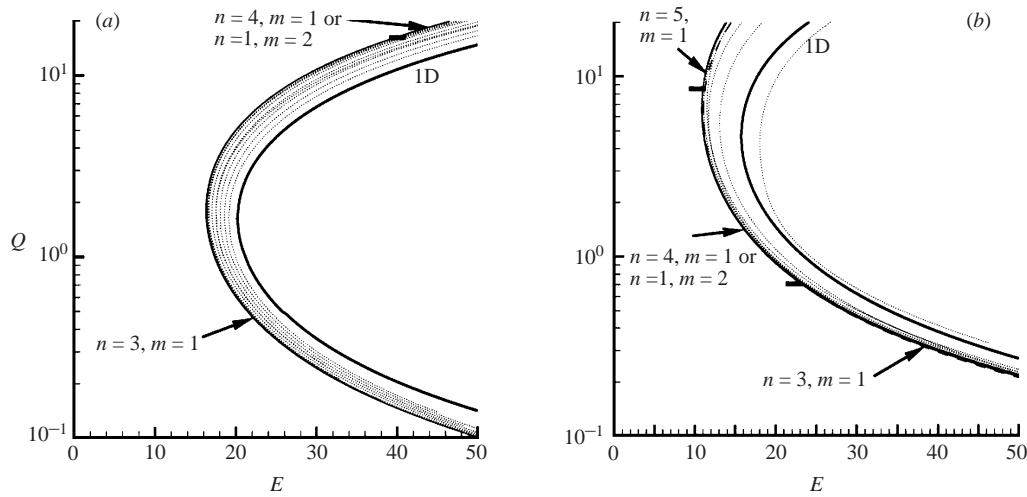


FIGURE 3. Neutral stability boundaries the (Q, E) -plane for spinning modes in a tube with diameter $d = 20$ at (a) $\gamma = 1.6$, (b) $\gamma = 1.3$.

cluttering we show only those curves which are in the neighbourhood of the leftmost boundary.

The main features of figures 3(a) and 3(b) are, first, that there exist spinning modes which are more unstable than (are to the left of) one-dimensional modes in the entire range of Q and E under investigation, and second, there exists a leftmost mode, perhaps different for different Q , such that all modes below and above it are less unstable. As we change Q , we may encounter bifurcations between different modes as indicated by the horizontal dashes in figure 3. In addition, note that many neutral stability curves are not far from the leftmost boundary, i.e. corresponding unstable

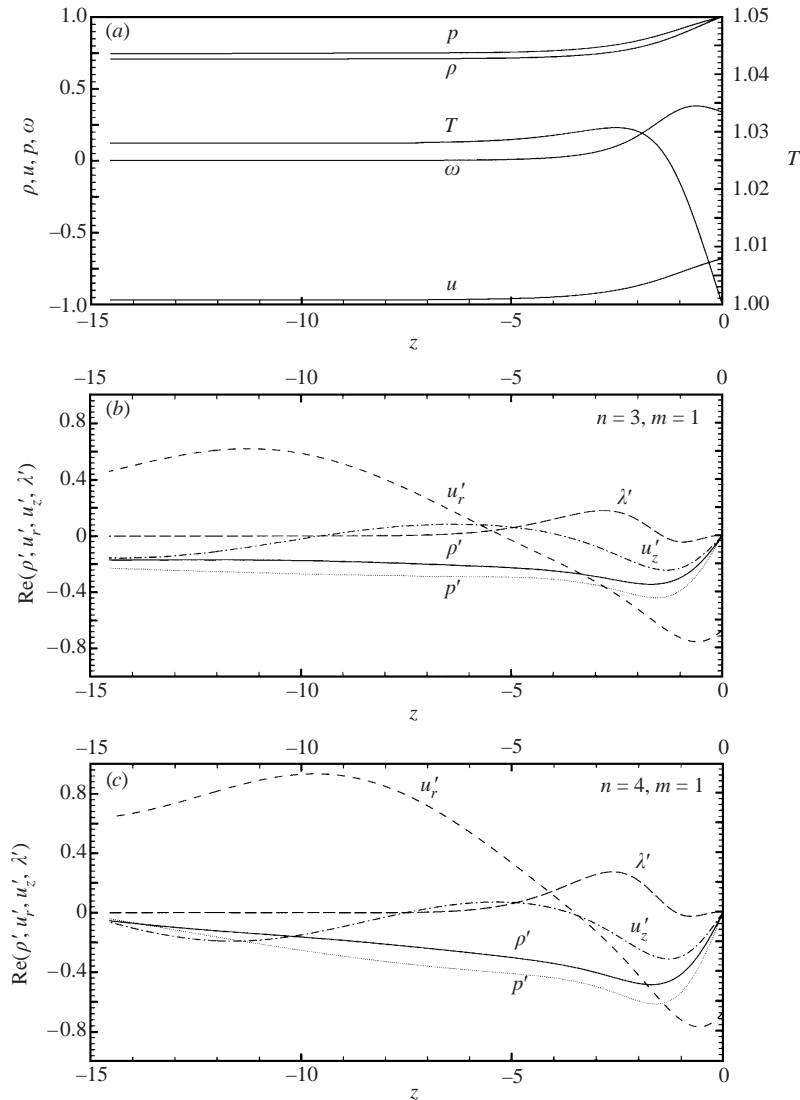


FIGURE 4. Steady-state profiles (a) and real parts of eigenfunctions, (b) and (c), at $Q = 0.69$, $E = 23.23$, $\gamma = 1.3$ and $d = 20$ (corresponds to the bifurcation point in figure 3b). In (b) and (c) the solid line is $\text{Re}(\rho')$, dashed $\text{Re}(u_r')$, dash-dot $\text{Re}(u_z')$, thin solid $\text{Re}(p')$ and long dash $\text{Re}(\lambda')$.

modes have a growth rate very close to the largest one. In fact, the larger the tube diameter the closer the neutral stability curves are to each other and many different modes will have growth rates near the maximum. In contrast, if the tube diameter is small, but still large enough so that spinning instability overtakes one-dimensional instability (see below), then the bifurcations are more pronounced.

Figure 4 shows the steady-state flow profiles and neutrally stable eigenfunctions corresponding to two leftmost modes $n = 3, m = 1$ and $n = 4, m = 1$ at the bifurcation value of $Q = 0.69$ and $E = 23.23$ in figure 3(b). The temporal frequencies of the two modes are $\text{Im}(\alpha) = 0.3798$ for $n = 3$ and $\text{Im}(\alpha) = 0.4499$ for $n = 4$. It is seen that there is little qualitative change in the behaviour of the eigenfunctions for the two modes, except the amplitudes are somewhat larger for $n = 4$ mode. The eigenfunctions

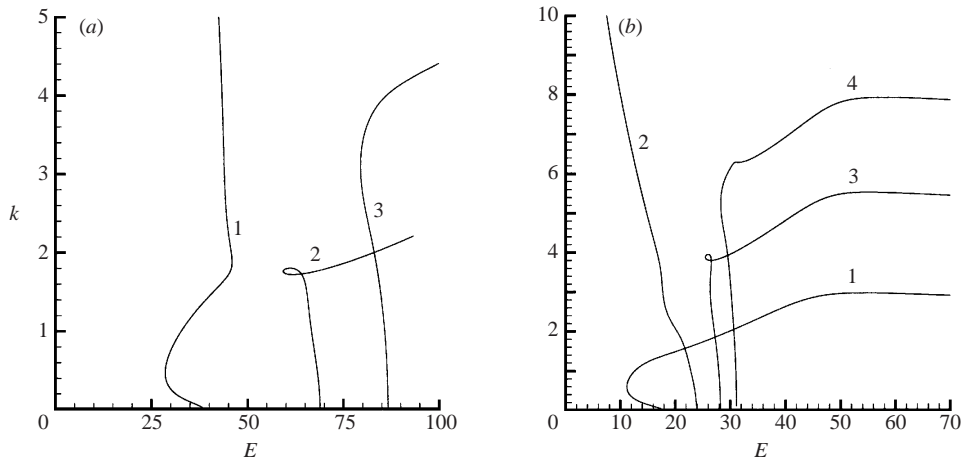


FIGURE 5. E, k neutral stability curves for the first few roots at $Q = 10$ and (a) $\gamma = 1.6$, (b) $\gamma = 1.3$.

shown in figures 4(a) and 4(c) are in fact only the axial amplitudes. The corresponding angular and radial parts reveal a significant change in the three-dimensional shape of the perturbation: $n = 3$ represents a wave with three crests in the azimuthal direction while there are four crests for the case with $n = 4$.

In order to find out behaviour of neutral stability curves for higher modes (hence larger k), we trace the neutrally stable roots as k is varied at some fixed Q . For example, we pick a value of $Q = 10$ in figure 3(a) and starting from the one-dimensional neutral stability curve ($k = 0$) calculate the dependence of E on k . The result is shown in figure 5(a). Figure 5(b) shows similar curves corresponding to figure 3(b). The numbering of the curves corresponds to the order in the temporal spectrum, i.e. 1 is the lowest frequency root, 2 is the next and so on. Several important conclusions can be drawn from these figures. First, the low- k behaviour which is shown in figures 3(a) and 3(b) with a distinct leftmost neutral stability boundary, terminates for the case with $\gamma = 1.3$ due to the mode $j = 2$ becoming more unstable at much larger k , and hence much larger n and m . This means that at $Q = 10$ and $\gamma = 1.3$ we have high-frequency instability dominant. This may be the reason for the experimental observation that when the mixture becomes more energetic (less dilute), the low-frequency spin detonation turns into a detonation with a 'rippled irregular front' (e.g. Munday *et al.* 1968; Duff 1961). (The peculiar behaviour of the second root in figure 5(a) and third root in figure 5(b) which exhibit loops is indicative of the complicated mathematical structure of the dispersion relation and is not of a numerical origin – hundreds of points are calculated along the loops alone, with tolerances on the order of 10^{-8} – 10^{-9} .) Note, that there is a region of smaller Q for which low-frequency instability prevails as figures 6(a) and 6(b) show. Thus at sufficiently small Q there is no high-frequency instability.

The case with $\gamma = 1.6$ does not show the high-frequency instability, at least in the reasonable range of k . (The reader should realize that this work can offer no guarantee that at much larger k we do not obtain again the high-frequency mode being the leftmost boundary, especially in view of the peculiarities of the dispersion relation. The reason is that it is prohibitively expensive to compute large- k limit, because the eigenfunctions become highly oscillatory – their frequency $\text{Im}(\alpha_i)$ grows linearly with k as $k \rightarrow \infty$. An asymptotic solution, similar to that of Erpenbeck 1966,

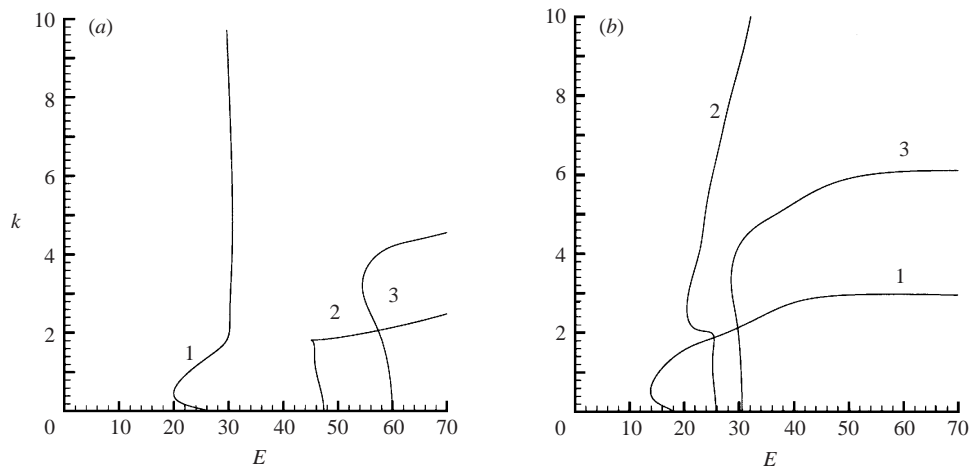


FIGURE 6. E, k neutral stability curves for the first few roots at (a) $Q = 5$, $\gamma = 1.6$, and (b) $Q = 2$, $\gamma = 1.3$.

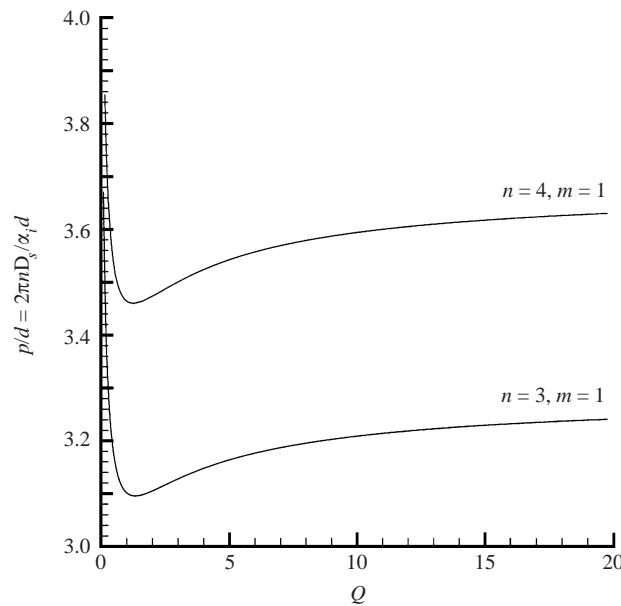


FIGURE 7. Pitch ratio p/d vs. the heat release Q along the neutral stability boundaries for $n = 3$, $m = 1$ and $n = 4$, $m = 1$ corresponding to figure 3(a), $\gamma = 1.6$, $d = 20$.

would in principle answer the question, but the analysis is rather involved and has yet to be satisfactorily resolved even for the simpler two-dimensional planar case). When the neutral stability boundary corresponds to the turning point for root 1 in figure 5(a), it means that there exists a specific wave shape, with specific $k = k_c$ (inverse of the radial wavelength), n_c (number of spinning heads), and m_c which has the maximum growth rate. From figure 5(a) we find $k_c = 0.45$ and from figure 3(a) $n_c = 3$ and $m_c = 1$.

Further support for the results having direct relevance to spin detonation is furnished by figure 7 which shows how the spin pitch to diameter ratio varies along the

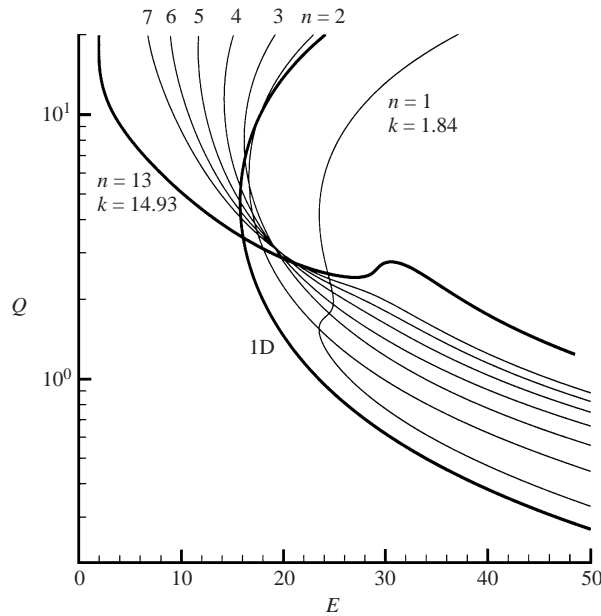


FIGURE 8. Stability behaviour of detonation in a small tube with diameter $d = 2$: Q, E neutral stability curves for modes $n = 1$ to $n = 13$ at $m = 1$ and $\gamma = 1.3$.

neutral stability curves in figure 3(a) for the modes with $n = 3$, $m = 1$ and $n = 4$, $m = 1$, which are the most unstable modes within the range of Q from 0 to 20. The ratio is calculated based on the temporal frequency $\alpha_i = \text{Im}(\alpha)$ of a neutrally stable root as

$$\frac{p}{d} = \frac{2\pi n D_s^*}{\alpha_i d}.$$

The predicted values are in good agreement with experiment with p/d being close to 3 for a low-frequency spin and being generally about 3 to 6 (cf. Gordon *et al.* 1959).

The values of p/d measured in experiments are for detonation with larger (non-linear) shock displacement than can be predicted simply from linear stability theory. And directly relating the frequencies of the *linear* perturbations to those of the actual nonlinear spin detonation is not entirely correct and the comparison is more properly regarded as an order of magnitude comparison. This caveat made, it is also worth pointing out that the pitch ratio is essentially determined by the imaginary part of the complex growth rate α_i . Research that dates back to Erpenbeck's original calculations of the frequency of unstable one-dimensional (galloping) detonation and comparison with Fickett and Wood's direct simulation, see Fickett & Davis (1979), have shown that the frequency of the instability from stability theory is often maintained as a feature of the large-amplitude manifestation of the instability. Many researchers have shown this subsequently in the past ten years (see e.g. Short & Quirk 1997).

Figure 8 shows the case of a small tube diameter $d = 2$ and $\gamma = 1.3$. First, note that the smallest radial wavenumber is now $k = 2x_{11}/d = 1.841$ and according to figure 5(b) there exists no part of the curve below $k = 1.841$, except a single point at $k = 0$, and hence no turning point region. That is why at sufficiently small Q the one-dimensional instability dominates, while at larger Q the high-frequency modes are more unstable. This result indicates that detonation of sufficiently dilute mixtures (small Q) in sufficiently small tubes would exhibit pulsating instability and

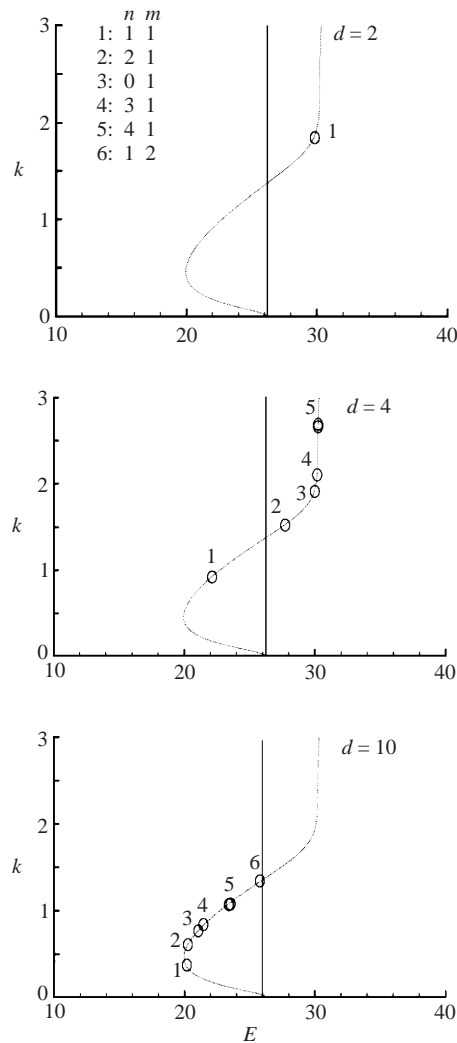


FIGURE 9. The effect of the tube diameter on the detonation stability at $Q = 5$, $\gamma = 1.6$.

thus lead to galloping detonation. This is also in agreement with experiment, see for example, Voitsekhovskii *et al.* (1963), Strehlow (1978), Fickett & Davis (1979), Vasiliev (1991).

Next we discuss what happens as we change various bifurcation parameters. Consider the effect of the tube diameter. The role of the tube diameter can be determined from E, k neutral stability diagrams. For example, consider the case shown in figure 6(a), which corresponds to a mixture with $Q = 5$ and $\gamma = 1.6$. The question we want to answer is: How does the most unstable mode change if the tube diameter is changed for a given explosive mixture? Do we observe bifurcations from one spinning mode to a different one if we change the tube diameter?

If we begin with a very small diameter d that corresponds to a pulsating ($k = 0$) instability and increase the diameter, then a sequence of bifurcations occurs from lower-mode spin to a higher-mode spin as shown in figure 9. The one-dimensional instability exists to the right of the vertical line in figure 9. The dotted curve is the E, k

neutral stability curve from figure 6(a). But for a finite tube diameter, the variations of k are discrete, and they are shown by circles, labelled 1, 2, 3, and so on, and their order corresponds to an increase in the neutrally stable modes with increasing radial wavenumber $k = 2x_{nm}/d$. At $d = 2$ the lowest spinning mode is $n = 1, m = 1$ (point 1 in figure 9) and corresponds to $k = 1.841$, and that point is to the right of the one-dimensional boundary, which means that in this tube the pulsating instability is dominant. As the tube diameter is increased to $d = 4$, the wavenumber k of the first spinning mode becomes equal to 0.92 and thus point 1 crosses the vertical line and becomes more unstable than the one-dimensional mode. Thus as the tube diameter is increased, the single-head spinning mode is more unstable than the pulsating mode. Note that all the remaining modes remain to the right of the vertical line and are less unstable than the $k = 0$ mode. However, if we increase the tube diameter further, more and more points cross the line and become more unstable than the one-dimensional mode. When the turning point is reached, the lower-frequency modes retreat to the right and start piling up at the origin of the vertical line at $k = 0$. At any fixed tube diameter, the mode which is leftmost corresponds to the most unstable mode. We find that the increase in tube diameter results in higher and higher modes being the most unstable.

Next consider the limit of a large tube diameter $d \rightarrow \infty$. In this limit the distance between neighbouring roots x_{nm} goes to zero, and hence we have a near-continuous variation of k . Still, figure 6(a) is in force with its turning point. Thus, no matter what the diameter is (if sufficiently large), there exists a characteristic radial wavenumber k_c (e.g. $k_c \approx 0.46$ at $Q = 5$ in figure 6a) for which the perturbation is most unstable. This corresponds to a certain pair of numbers n, m dependent on d (which can be found from $x_{nm} = k_c d/2$); however we emphasize that the wavelength in the radial direction becomes *independent* of d as $d \rightarrow \infty$, as it clearly should. At large $k_c r$ the Bessel function $J_n(k_c r)$ can be approximated by its asymptotic form $J_n(k_c r) \sim \sqrt{2/(\pi k_c r)} \cos(k_c r - \pi n/2 - \pi/4)$, from which it is clear that the characteristic wavelength of the most unstable mode is $\lambda_c = 2\pi/k_c \approx 13.7$. Thus, we conclude that the transverse cell size is about 14 times the size of the reaction zone at these particular values of $Q = 5$ and $\gamma = 1.6$. In general, we expect k_c to be a function of Q and γ , and thus we can write that

$$\tilde{\lambda}_c = \frac{2\pi}{k_c(Q, \gamma)} \tilde{l}_{1/2}.$$

The value of $k_c(Q, \gamma)$ can be determined from the stability analysis, $\tilde{l}_{1/2}$ is determined by the kinetics and thermodynamic properties of the mixture.

It is interesting to compare the wavelength predicted by the above formula with experiment and numerical calculations. If we take the data from the detonation database at Caltech (Kaneshige, Shepherd & Teodorczyk 1997), and the steady reaction-zone length calculated using the detailed chemical mechanism, we have the following data for $2\text{H}_2 + \text{O}_2 + 26\text{Ar}$ (90%Ar): in the fresh mixture $\gamma_0 = 1.64$, in the von Neumann state $\gamma_{vN} = 1.6$, effective heat release and activation energy are $Q \approx 7$ and $E \approx 34$, respectively. The experimental value of the cell width λ_w is about 40 mm and the length of the reaction zone l_{rz} (based on maximum temperature gradient) is 1.23 mm. Their ratio gives $\lambda_w/l_{rz} = 33$, which differs from that predicted by the linear analysis by about a factor of 2. The difference can be attributed to many factors, for example to the ambiguities in the definitions of various quantities such as the effective activation energy E and γ . But this comparison should be regarded as an order of

magnitude comparison and in that sense the agreement is good. More accurate and careful comparison can be made.

Dilution affects the stability characteristics most significantly through its relationship to the heat release Q and γ . If the diluent is a monatomic gas, then we expect large values for γ . Lighter diluents such as helium would also increase the sound speed \tilde{c}_0 in the fresh mixture, thus Q , which is non-dimensionalized with respect to \tilde{c}_0^2/γ , will be small not only because of dilution, but also due to the large sound speed in the mixture. Thus in a wide range of dilutions for helium-diluted mixtures, the low-frequency spin can be expected. Heavier diluents, especially polyatomic, would result in smaller γ as well as larger Q , which both correspond a large number of high-frequency unstable modes and thus would favour irregular detonation fronts. We can see in figures 3(a) and 3(b) that as Q is increased, which can be due to decrease in dilution, there are bifurcations from lower- to higher-frequency branches.

Now let us discuss what the effect of mixture initial pressure is on the spin detonation. One of the ways the spin detonation is observed experimentally is by lowering the initial pressure p_0 of a mixture in a tube of fixed diameter and at fixed mixture composition. As the pressure is decreased, a cellular detonation transforms into spin detonation after the cell size, which increases with decrease in pressure, becomes comparable to the tube diameter. The effect of the initial pressure p_0 of a fresh mixture cannot be directly calculated in our model and has to be inferred from other results. The reason is that p_0 is absent in the model entirely due to the first order of the reaction rate, but since typically for realistic kinetics the length of the reaction zone is inversely proportional to p_0 , the variations of the initial pressure can be related to those of the reaction zone. For example, if $\tilde{l}_{1/2} \sim 1/p_0$, then the non-dimensional tube diameter $d = \tilde{d}/\tilde{l}_{1/2} \sim \tilde{d}p_0$. Hence lowering p_0 at fixed \tilde{d} is equivalent to decreasing \tilde{d} at fixed p_0 and so we can infer the role of the initial pressure from the effect of the tube diameter. In fact, p_0 plays a more complex role as its variation shifts the equilibrium composition of detonation products with an accompanying change in the heat effect and detonation velocity. However those dependences are beyond the scope of the constitutive model used in this study.

8. Conclusions

We have investigated the instability of a one-dimensional detonation wave propagating in a cylindrical tube to three-dimensional linear perturbations using the normal mode approach. The instability spectra are calculated exactly using a high-accuracy ODE solver for the eigenfunctions and a Newton–Raphson root solver for the radiation condition. The analysis shows the existence of spinning unstable modes and bifurcations from lower-frequency spin to higher-frequency spin as the mixture becomes more energetic with larger heat release Q . The behaviour of the unstable modes with respect to the variations of the bifurcation parameters of the problem strongly supports the possibility of the spinning instability being at the origin of the well-known spin detonation.

This work was supported by the US Air Force Office of Scientific Research (F49620-00-1-0005, program manager Dr Arje Nachman). Additional support was provided by the US Air Force Research Laboratory Munitions Directorate, Eglin AFB (F08630-00-1-0002). A. R. K. is grateful to Professor M. Short for help with code verification and for discussions about detonation stability.

Appendix A. Definition of $\mathbf{A}_z, \mathbf{A}_r, \mathbf{A}_\theta, \mathbf{a}, \mathbf{B}_r, \mathbf{B}_\theta, \mathbf{b}, \mathbf{c}$

The following square matrices and column vectors are used to write the governing equations in shock-attached coordinates in vector form:

$$\mathbf{A}_z = \begin{bmatrix} u_z & 0 & 0 & \rho & 0 & 0 \\ 0 & u_z & 0 & 0 & 0 & 0 \\ 0 & 0 & u_z & 0 & 0 & 0 \\ 0 & 0 & 0 & u_z & 1/(\gamma\rho) & 0 \\ 0 & 0 & 0 & \gamma p & u_z & 0 \\ 0 & 0 & 0 & 0 & 0 & u_z \end{bmatrix}, \quad \mathbf{A}_r = \begin{bmatrix} u_r & \rho & 0 & 0 & 0 & 0 \\ 0 & u_r & 0 & 0 & 1/(\gamma\rho) & 0 \\ 0 & 0 & u_r & 0 & 0 & 0 \\ 0 & 0 & 0 & u_r & 0 & 0 \\ 0 & \gamma p & 0 & 0 & u_r & 0 \\ 0 & 0 & 0 & 0 & 0 & u_r \end{bmatrix}, \quad (\text{A } 1)$$

$$\mathbf{A}_\theta = \begin{bmatrix} u_\theta & 0 & \rho & 0 & 0 & 0 \\ 0 & u_\theta & 0 & 0 & 0 & 0 \\ 0 & 0 & u_\theta & 0 & 1/(\gamma\rho r) & 0 \\ 0 & 0 & 0 & u_\theta & 1/(\gamma\rho) & 0 \\ 0 & 0 & 0 & \gamma p & u_\theta & 0 \\ 0 & 0 & 0 & 0 & 0 & u_\theta \end{bmatrix}, \quad \mathbf{a}_r = \begin{bmatrix} \rho u_r \\ -u_\theta/r \\ u_r u_\theta/r \\ 0 \\ 0 \\ 0 \end{bmatrix}. \quad (\text{A } 2)$$

$$\mathbf{B}_r = \begin{bmatrix} u_r & \rho & 0 & 0 & 0 & 0 \\ 0 & u_r & 0 & 0 & 1/(\gamma\rho) & 0 \\ 0 & 0 & u_r & 0 & 0 & 0 \\ 0 & 0 & 0 & u_r & 0 & 0 \\ 0 & \gamma p & 0 & 0 & u_r & 0 \\ 0 & 0 & 0 & 0 & 0 & u_r \end{bmatrix}, \quad \mathbf{B}_\theta = \begin{bmatrix} u_\theta & 0 & \rho & 0 & 0 & 0 \\ 0 & u_\theta & 0 & 0 & 0 & 0 \\ 0 & 0 & u_\theta & 0 & 1/(\gamma\rho) & 0 \\ 0 & 0 & 0 & u_\theta & 0 & 0 \\ 0 & 0 & \gamma p & 0 & u_\theta & 0 \\ 0 & 0 & 0 & 0 & 0 & u_\theta \end{bmatrix}, \quad (\text{A } 3)$$

$$\mathbf{b} = \begin{bmatrix} 0 \\ 0 \\ 0 \\ 1 \\ 0 \\ 0 \end{bmatrix}, \quad \mathbf{c} = \begin{bmatrix} 0 \\ 0 \\ 0 \\ 0 \\ (\gamma - 1)\rho\beta\omega \\ \omega \end{bmatrix}. \quad (\text{A } 4)$$

Appendix B. Radiation condition including perturbations of the reaction rate

If we separate the angular and radial dependences of the perturbations as in equations (23) and (25) and use the relationship $\hat{u}_\theta = in\hat{u}_r$, then we obtain the following acoustic system in the amplitudes of perturbations depending only on t and z :

$$\frac{\partial \hat{u}_r}{\partial t} + u_b \frac{\partial \hat{u}_r}{\partial z} + \frac{\hat{p}}{\gamma \rho_b} = 0, \quad (\text{B } 1)$$

$$\frac{\partial \hat{u}_z}{\partial t} + u_b \frac{\partial \hat{u}_z}{\partial z} + \frac{1}{\gamma \rho_b} \frac{\partial \hat{p}}{\partial z} + \frac{\partial^2 \hat{\psi}}{\partial t^2} = 0, \quad (\text{B } 2)$$

$$\frac{\partial \hat{p}}{\partial t} + u_b \frac{\partial \hat{p}}{\partial z} + \gamma p_b \left(\frac{\partial \hat{u}_z}{\partial z} - k^2 \hat{u}_r \right) - (\gamma - 1)\beta \rho_b \omega_z^b \hat{\lambda} = 0. \quad (\text{B } 3)$$

Note, that since the continuity equation is the only one containing the density perturbation, it is not needed in the following analysis. Also, $\partial^2 \hat{\psi} / \partial t^2$ can always be absorbed into \hat{u}_z so that $\hat{u}_z \rightarrow \hat{u}_z + \partial \hat{\psi} / \partial t$ and the equations retain their form, hence it will be dropped in the following derivations. Here $\hat{\lambda} = \exp(\alpha t + k_z z)$ is the Fourier component of the solution of the equation for $\hat{\lambda}$.

The above system can be written in matrix form as

$$\frac{\partial \mathbf{f}}{\partial t} + \mathbf{A} \cdot \frac{\partial \mathbf{f}}{\partial z} + \mathbf{B} \cdot \mathbf{f} = \mathbf{b} \hat{\lambda}, \quad (\text{B } 4)$$

where locally we define

$$\mathbf{f} = \begin{bmatrix} \hat{u}_r \\ \hat{u}_z \\ \hat{p} \end{bmatrix}, \quad \mathbf{A} = \begin{bmatrix} u_b & 0 & 0 \\ 0 & u_b & \frac{1}{\gamma \rho_b} \\ 0 & \gamma \rho_b c_b^2 & u_b \end{bmatrix},$$

$$\mathbf{B} = \begin{bmatrix} 0 & 0 & \frac{1}{\gamma \rho_b} \\ 0 & 0 & 0 \\ -\gamma \rho_b k^2 c_b^2 & 0 & 0 \end{bmatrix}, \quad \mathbf{b} = \begin{bmatrix} 0 \\ 0 \\ a_0 \end{bmatrix} \quad (\text{B } 5)$$

and $a_0 = (\gamma - 1) \beta \rho_b \omega_{\lambda}^b$, $c_b^2 = p_b / \rho_b$, $\alpha = \omega_{\lambda}^b - k_z u_b$. The system (B 4) can be diagonalized if written in terms of the Riemann invariants $r_i = \mathbf{l}_i \cdot \mathbf{f}$, i.e. the dot products of the left-hand eigenvectors of the matrix \mathbf{A} and the vector \mathbf{f} . The eigenvectors are

$$\mathbf{l}_1 = [0, \gamma \rho_b c_b, 1], \quad \mathbf{l}_2 = [1, 0, 0], \quad \mathbf{l}_3 = [0, -\gamma \rho_b c_b, 1]. \quad (\text{B } 6)$$

Then we obtain $\mathbf{l}_i \cdot \mathbf{A} = m_i \mathbf{l}_i$ with

$$m_1 = u_b + c_b, \quad m_2 = u_b, \quad m_3 = u_b - c_b, \quad (\text{B } 7)$$

and the diagonalized system in r_i becomes

$$\frac{\partial r_i}{\partial t} + m_i \frac{\partial r_i}{\partial z} + b_{1i} = b_{2i} \hat{\lambda} \quad \text{for } i = 1, 2, 3, \quad (\text{B } 8)$$

where

$$\mathbf{r} = \begin{bmatrix} \hat{p} + \gamma \rho_b c_b \hat{u}_z \\ \hat{u}_r \\ \hat{p} - \gamma \rho_b c_b \hat{u}_z \end{bmatrix}, \quad \mathbf{b}_1 = \mathbf{l} \cdot \mathbf{B} \cdot \mathbf{f} = \begin{bmatrix} -\gamma \rho_b c_b^2 k^2 \hat{u}_r \\ \hat{p} \\ \gamma \rho_b \\ -\gamma \rho_b c_b^2 k^2 \hat{u}_r \end{bmatrix}, \quad \mathbf{b}_2 = \mathbf{l} \cdot \mathbf{b} = \begin{bmatrix} a_0 \\ 0 \\ a_0 \end{bmatrix}. \quad (\text{B } 9)$$

If we denote $L_+ = \partial / \partial t + (u_b + c_b) \partial / \partial z$, $L_- = \partial / \partial t + (u_b - c_b) \partial / \partial z$, and $L_0 = \partial / \partial t + u_b \partial / \partial z = \frac{1}{2}(L_+ + L_-)$, the equations for r_i can be written in expanded form as

$$L_+(r_1) - \gamma \rho_b c_b^2 k^2 r_2 = a_0 \hat{\lambda}, \quad (\text{B } 10)$$

$$L_0(r_2) + \frac{1}{2\gamma \rho_b} (r_1 + r_3) = 0, \quad (\text{B } 11)$$

$$L_-(r_3) - \gamma \rho_b c_b^2 k^2 r_2 = a_0 \hat{\lambda}. \quad (\text{B } 12)$$

If we take L_- of (B 10), L_+ of (B 12), add them, and make use of (B 11), we obtain a single equation in $r_1 + r_3 = 2\hat{p}$, which is the non-homogeneous Klein–Gordon equation,

$$\frac{\partial^2 \hat{p}}{\partial t^2} + 2u_b \frac{\partial^2 \hat{p}}{\partial t \partial z} - (c_b^2 - u_b^2) \frac{\partial^2 \hat{p}}{\partial z^2} + (c_b k)^2 \hat{p} - a_0 \omega_{,\lambda}^b e^{\alpha t + k_z z} = 0. \quad (\text{B } 13)$$

The solution of this equation is

$$\hat{p} = A_1 e^{\alpha t + s z} + A_0 e^{\alpha t + k_z z}, \quad (\text{B } 14)$$

where A_1 is an unknown constant, $A_0 = a_0 \omega_{,\lambda}^b / ((\omega_{,\lambda}^b)^2 + (k^2 - k_z^2) c_\infty^2)$. The complex wavenumber s is given by equation (37) and satisfies the boundedness condition as discussed in the main text above.

If we now add equations (B 10) and (B 12) and write L_+ and L_- explicitly, we obtain the following equation:

$$\frac{\partial \hat{p}}{\partial t} + u_b \frac{\partial \hat{p}}{\partial z} + \gamma \rho_b c_b^2 \frac{\partial \hat{u}_z}{\partial z} - \gamma \rho_b c_b^2 k^2 \hat{u}_r = a_0 \hat{\lambda}. \quad (\text{B } 15)$$

We separate the exponential time dependence as $\hat{p} = p' \exp(\alpha t)$ and so on, to obtain

$$\alpha p' + u_b \frac{dp'}{dz} + \gamma \rho_b c_b^2 \frac{du'_z}{dz} - \gamma \rho_b c_b^2 k^2 u'_r = a_0 \lambda'. \quad (\text{B } 16)$$

Differentiating (B 14) we obtain

$$\frac{dp'}{dz} = s(p' - A_0 \lambda') + A_0 k_z \lambda'. \quad (\text{B } 17)$$

Inserting this expression into (B 16) we obtain the general radiation condition

$$\frac{du'_z}{dz} - k^2 u'_r + \frac{\alpha + s u_b}{\gamma \rho_b c_b^2} p' - \mu \lambda' = 0, \quad (\text{B } 18)$$

where

$$\mu = \frac{\gamma - 1}{\gamma} \frac{\beta \omega_{,\lambda}^b}{c_b^2} \left[1 + \frac{\omega_{,\lambda}^b (s - k_z)}{(\omega_{,\lambda}^b)^2 + (k^2 - k_z^2) c_b^2} \right] \quad (\text{B } 19)$$

and $k_z = (\omega_{,\lambda}^b - \alpha) / u_b$.

In some previous studies the term proportional to λ' has been dropped on the grounds of its presumed exponential smallness in the burnt region. It is clear from (B 19) that $\mu = O(\omega_{,\lambda}^b) = O(k \exp(-\Theta / c_b^2))$, provided that other factors, including the term in the square bracket are $O(1)$. The function $\lambda'(z)$ decays exponentially to zero as $z \rightarrow -\infty$ since then $\lambda' \sim \exp(k_z z) \sim \exp(\text{Re}(k_z) z)$ and $\text{Re}(k_z) = -(\alpha_r - \omega_{,\lambda}^b) / u_b > 0$. Thus the assumption is justified provided $\mu = O(1)$, which is true at finite values of Θ .

Reduction of the radiation condition (B 18) to the one-dimensional case can be done through integration of (B 18) over z at $k = 0$ and shows that it is exactly the same condition as given in Lee & Stewart (1990). One should only keep in mind that $\int (du'_z / dz) dz = u'_z + \alpha$ which is due to the difference in definitions of u_z .

REFERENCES

- BONE, W. A., FRASER, R. P. & WHEELER, W. H. 1935 Photographic investigations of flame movements in gaseous explosions. Part VII – the phenomenon of spin in detonations. *Phil. Trans. R. Soc. Lond. A* **235**, 29–68.

- BOURLIOUX, A. & MAJDA, A. J. 1992 Theoretical and numerical structure for unstable two-dimensional detonations. *Combust. Flame* **90**, 211–229.
- BOURLIOUX, A. & MAJDA, A. J. 1995 Theoretical and numerical structure of unstable detonations. *Phil. Trans. R. Soc. Lond. A* **350**, 29–68.
- BUCKMASTER, J. D. & LUDFORD, G. S. S. 1986 The effect of structure on the stability of detonations I. Role of the induction zone. In *Twenty-first Symp. (Intl) on Combustion*, pp. 1669–1676. The Combustion Institute.
- CAMPBELL, C. & WOODHEAD, D. W. 1926 The ignition of gases by an explosion wave. I. Carbon monoxide and hydrogen mixtures. *J. Chem. Soc.* **129**, 3010–3021.
- CAMPBELL, C. & WOODHEAD, D. W. 1927 Striated photographic records of explosion waves. *J. Chem. Soc.* **130**, 1572–1578.
- CHU, B. T. 1956 Vibration of the gaseous column behind a strong detonation wave. In *Gas Dynamics Symposium on Aerothermochemistry*. Northwestern University Press, Evanston.
- DUFF, R. E. 1961 Investigation of spinning detonation and detonation stability. *Phys. Fluids* **4**, 1427–1433.
- ERPENBECK, J. J. 1962 Stability of steady-state equilibrium detonations. *Phys. Fluids* **5**, 604–614.
- ERPENBECK, J. J. 1964 Stability of idealized one-reaction detonations. *Phys. Fluids* **7**, 684–696.
- ERPENBECK, J. J. 1966 Detonation stability for disturbances of small transverse wavelength. *Phys. Fluids* **9**, 1293–1306.
- FAY, J. A. 1952 A mechanical theory of spinning detonation. *J. Chem. Phys.* **20**, 942–950.
- FICKETT, W. & DAVIS, W. C. 1979 *Detonation*. University of California Press.
- GORDON, W. E., MOORADIAN, A. J. & HARPER, S. A. 1959 Limit and spin effects in hydrogen-oxygen detonations. In *Seventh Symp. (Intl) on Combustion*, pp. 752–759. The Combustion Institute.
- KANESHIGE, M., SHEPHERD, J. E. & TEODORCZYK, A. 1997 Detonation database at Explosion Dynamics Laboratory, Caltech. <http://www.galcit.caltech.edu/EDL/>.
- LEE, H. I. & STEWART, D. S. 1990 Calculation of linear detonation instability: one-dimensional instability of plane detonation. *J. Fluid Mech.* **212**, 103–132.
- MANSON, N. 1946 On the structure of so-called helical detonation waves in gaseous mixtures. *C. r. hebdom. Acad. Sci. Paris* **222**, 46–51.
- MATKOWSKY, B. J. & OLAGUNJU, D. O. 1982 Spinning waves in gaseous combustion. *SIAM J. Appl. Maths* **42**, 1138–1156.
- MUNDAY, G., UBBELOHDE, A. R. & WOOD, I. F. 1968 Fluctuating detonations in gases. *Proc. R. Soc. Lond. A* **306**, 171–178.
- NIST 2001 Mathematical software repository, <http://gams.nist.gov>.
- PUKHNACHEV, V. V. 1963 The stability of Chapman-Jouguet detonations. *Sov. Phys. Dokl.* **8** (4), 338–340.
- SCHOTT, G. L. 1965 Observations of the structure of spinning detonation waves. *Phys. Fluids* **8**, 850–865.
- SHORT, M. & QUIRK, J. J. 1997 On the nonlinear stability and detonability limit of a detonation wave for a model 3-step chain-branching reaction. *J. Fluid Mech.* **339**, 89–119.
- SHORT, M. & STEWART, D. S. 1998 Cellular detonation stability. Part 1. A normal-mode linear analysis. *J. Fluid Mech.* **368**, 229–262.
- SIVASHINSKY, G. 1981 On spinning propagation of combustion waves. *SIAM J. Appl. Maths* **40**, 432–438.
- STRELOW, R. A. 1978 *Fundamentals of Combustion*. Kreiger.
- VASILIEV, A. A. 1991 The limits of stationary propagation of gaseous detonation. In *Dynamic Structure of Detonations in Gaseous and Dispersed Media* (ed. A. A. Borisov). Kluwer.
- VOITSEKHOVSKII, B. V., MITROFANOV, V. V. & TOPCHIAN, M. Y. 1963 *Struktura Fronta Detonatsii v Gasakh*. Akad. Nauk SSSR. Translation: 1966 *The Structure of Detonation Fronts in Gases*. Report FTD-MTD-64-527, Foreign Technology Division, Wright Patterson Air Force Base, Ohio (AD 633–821).
- YAO, J. & STEWART, D. S. 1996 On the dynamics of multi-dimensional detonation waves. *J. Fluid Mech.* **309**, 225–275.
- ZHANG, F. & GRONIG, H. 1991 Spin detonation in reactive particles-oxidizing gas flow. *Phys. Fluids A* **3**, 1983–1990.